Proceedings of ASME Turbo Expo 2011
GT2011
June 6-10, 2011, Vancouver, British Columbia, Canada

GT2011-45397

EXPERIMENTAL COMPARISON OF DBD PLASMA ACTUATORS FOR LOW REYNOLDS NUMBER SEPARATION CONTROL

Christopher Marks **Rolf Sondergaard** **Mitch Wolff** **Rich Anthony**

U.S. Air Force Research Laboratory, Propulsion Directorate
Wright Patterson AFB, OH 45433, USA

ABSTRACT

This paper presents experimental work comparing several Dielectric Barrier Discharge (DBD) plasma actuator configurations for low Reynolds number separation control. Actuators studied here are being investigated for use in a closed loop separation control system. The plasma actuators were fabricated in the U. S. Air Force Research Laboratory Propulsion Directorate's thin film laboratory and applied to a low Reynolds number airfoil that exhibits similar suction surface behavior to those observed on Low Pressure (LP) Turbine blades. In addition to typical asymmetric arrangements producing downstream jets, one electrode configurations was designed to produce an array of off axis jets, and one produced a spanwise array of linear vertical jets in order to generate vorticity and improved boundary layer to freestream mixing. The actuators were installed on an airfoil and their performance compared by flow visualization, surface stress sensitive film (S3F), and drag measurements. The experimental data provides a clear picture of the potential utility of each design. Experiments were carried out at four Reynolds numbers, $1.4x10^5$, 1.0×10^5, 6.0×10^4, and 5.0×10^4 at a -1.5° angle of attack. Data was taken at the AFRL Propulsion Directorate's Low Speed Wind Tunnel (LSWT) facility.

INTRODUCTION

The environment in a low pressure (LP) turbine at high altitude can reach Reynolds numbers below 25,000 [15]. Highly loaded blades with large turning angles are prone to flow separation and reduced efficiency at low Reynolds number. Researchers have studied different active and passive flow control techniques to increase the efficiency of the turbine blades at low Reynolds number – see summary by Rivir et al. in 2004 [17]. Dielectric Barrier Discharge (DBD) plasma actuators used in this paper are a low power, active separation control method. The work presented here is part of an effort to develop a laboratory level Low Reynolds number closed loop separation control system. The DBD plasma actuators configurations evaluated are being considered as an additional alternative to other actuation methods being studied.

In order to most efficiently use a plasma actuator as a separation control method, it is important to understand the mechanism by which a separated boundary layer can be reattached or forced into early transition. With respect to control of turbine blades, Rivir et al. points out that successful techniques have introduced longitudinal or streamwise vortices which "reenergize the wall boundary layer flow by entraining and redistributing momentum from the primary flow to the wall layer" [17]. Three different methods of controlling highly loaded LP turbine blades have been demonstrated in a low speed linear cascade at the AFRL Low Speed Wind Tunnel (LSWT) facility that introduce streamwise vorticity. Passive separation control was demonstrated by Lake [1] using dimples applied to the suction surface of the Pack-B LP turbine profile. Flow visualization by Mahmood et al. [2] showed that dimples act as a vortex generator, introducing multiple longitudinal vortices. The use of steady and pulsed vortex generator jets (VGJ) were demonstrated by Sondergaard et al. [3] and Bons et al. [4] to reattach low Reynolds number separated flow. An aggressive skew angle relative to the freestream of 45-90 degrees resulted in one strong slow decaying longitudinal vortice that was shown by Johnston et al [5] to be more effective at transferring momentum from the freestream to the wall.

Dielectric barrier discharge (DBD) plasma actuators have also been used in a number of LP turbine separation control studies [18][19][20][21][35], and are typically a single asymmetric spanwise plasma actuator which pulls high momentum fluid from the freestream into the boundary layer. Pulsed actuator operation has been shown to generate spanwise coherent vortical structures that are more effective at transferring momentum to the boundary layer while using less power [19][21]. In each of these approaches the actuators acted as an instability generating mechanism.

The objective of this study was to verify that the DBD plasma actuator could control the flow over an Eppler 387 (E387) airfoil at Low Reynolds number, and evaluate the capability of three different electrode configurations for use in a Low Reynolds number separation control system. The uniqueness of this study is the head to head comparison of three different DBD plasma actuator electrode configurations. Two different electrode arrangements were compared to an asymmetric spanwise electrode arrangement in hopes of generating increased control authority by generating streamwise vorticity. The E387 was chosen because the suction surface flowfield was similar to previous LP turbine blade design at low Reynolds number tested in the U.S. Air Force Research Laboratory Propulsion Directorate (LSWT) facility. The E387 airfoil allowed the use of a straight section wind tunnel rather than linear cascade, and simplified optical access, setup, and mounting of the S3F sensor to the airfoil.

Application of DBD to Low Pressure Turbine Blades

The standard configuration of an asymmetric DBD with the electrode interface mounted perpendicular to the flow direction has been shown to entrain momentum from the primary flow into the wall layer (see Figure 2) [43]. A perpendicular orientation to the primary flow has been demonstrated to reattach a separated LP turbine boundary layer at low Reynolds number by a number of researchers described below.

List et al. in 2003 [35] applied a single DBD plasma actuator for control of laminar separation of a linear cascade of Langston turbine blades in which a laminar separation bubble was observed at low Reynolds numbers ($Re=3.0x10^4$ & $7.4x10^4$). A DBD plasma actuator was placed just upstream of the separation location and voltage was increased until the separation bubble was eliminated.

Huang et al. published two papers, the first in 2003 [18] and the second in 2006 [19] that investigated the use of a single DBD plasma actuator applied to a linear cascade of Pack-B LP turbine blades for flow control.

The first work focused on identifying the flowfield around the Pack-B blade in a linear cascade wind tunnel and comparing the use of a single DBD plasma actuator and vortex generator tabs to control the suction surface laminar flow separation. The authors placed one spanwise actuator upstream of the separation line with electrodes mounted perpendicular to flow direction creating a two dimension steady wall jet. The actuators shifted reattachment location upstream. The authors noted a threshold driving voltage amplitude at which a further increase in applied voltage would yield very little movement of reattachment point [18].

The second paper of Huang et al. [19] compared the use of steady AC driving waveform versus unsteady AC driving waveform for separation control of the Pack-B. They found both unsteady and steady actuators to be effective, but labeled the unsteady actuator the more effective of the two. Huang et al. suggests the steady actuators are turbulence tripping, and the unsteady actuators generate a train of spanwise structures that promote mixing. The optimum excitation frequency for the unsteady actuators to reattach flow was at a Strouhal number equal to unity. The Strouhal number was calculated based on length of separated zone and local freestream velocity.

Rizzetta and Visbal [20][21] performed a computational study focusing on the identification of effective strategies for separation control of highly loaded low pressure turbine blades. Numerical simulations were performed on a simulated Pack-B blade set. The actuators were modeled by momentum addition and the model did include the actual actuator physics. Both steady and unsteady actuators were examined, with the unsteady actuators introducing unsteady forcing. Co-flow and counter-flow configurations were evaluated. The computational study indicated higher power levels exerted greater control, pulsed excitation was more effective than continuous actuation due to enhanced mixing, and the pulsed counter-flow actuator configuration provided the most effective control with the least expenditure of energy [20].

DBD Plasma Actuator Background and Overview

A simple schematic of an asymmetric configuration of DBD is shown in Figure 1. This configuration has been studied significantly in recent literature.

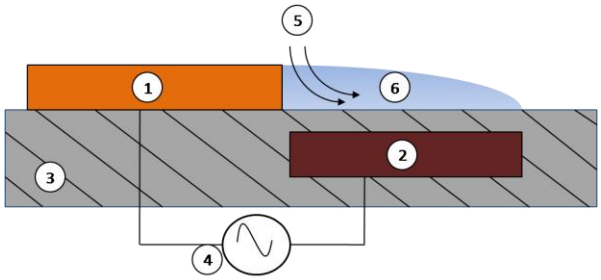

Figure 1. Asymmetric configuration of DBD plasma actuator.

The encapsulated electrode is typically grounded and the voltage potential is alternated between positive and negative. Typically high voltage AC is applied to the electrodes with voltage amplitudes of several kV_{p-p} to tens of kV_{p-p} and frequencies from around 1 kHz to tens of kilohertz. For detailed information and background on the physics of the plasma discharge readers should refer to other papers [7]-[9], the topical review paper by Fridman et al. [12] and a paper by Moreau [1].

An electrostatic force of Equation 1[8], acts in the charged species located in the plasma which results in an electric wind or induced velocity, in the form of a wall jet.

$$\vec{F} = \rho_e \vec{E} = -(\varepsilon_0/\gamma_D^2)\phi\vec{E} \quad (1)$$

In equation 1, ρ_e is the net charge density, E is the electric field, ε_0 is the permittivity of free space,and γ_D is the debye length. The thrust produced by the force has been reported to be in the range of 10 mN or less [9]. The induced air flow can be several

meters per second, but larger velocities have been generated [1]. An induced velocity and low power requirement make a DBD plasma actuator a viable candidate for low speed flow control applications. The use of DBD plasma actuators in a LP turbine will require additional research including operation in a harsh environment, scaling to higher Mach number flows, and reliability.

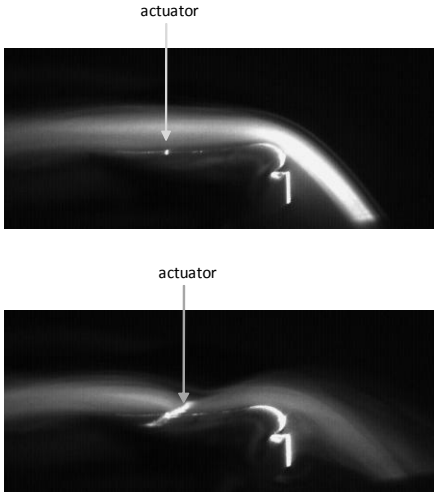

Figure 2. Visualization of the induced velocity generated by a DBD plasma actuator single asymmetric electrode configuration. Top image: actuator off. Bottom image: actuator on. Flow is from left to right.

Alternate DBD Plasma Actuator Configurations

A majority of fundamental research and application of DBD plasma actuators for flow control has utilized the linear asymmetric electrode arrangement illustrated in Figure 1. This configuration generates an induced velocity in the form of thin wall jet pointing downstream over the buried electrode. This configuration is effective at reenergizing the boundary layer by transferring momentum from the freestream to the boundary layer. The height of the jet is typically only several millimeters above the surface [11]. As mentioned above this configuration was used experimentally by Huang et al. to reattach and decrease the length of a separation bubble over the Pack-B airfoil. The jet was oriented downstream along the surface of the airfoil just upstream from separation adding momentum to the boundary layer with the objective of overcoming the adverse pressure gradient aft of the negative pressure peak. Huang et al. concluded the actuator acted as a turbulent trip, promoting earlier transition to turbulent boundary layer [19]. A nearly analogous computational study by Rizzetta and Visbal found the same steady actuator configuration mounted facing upstream more effective then the downstream facing plasma actuator. They predicted that the upstream jet created a local small scale separation and subsequent formation of vorticity and turbulent mixing [21]. It should be noted that both Huang et al. and Rizzetta and Visbal investigated pulsed configurations in their studies and found them to be more effective while using less power. Their performance gain was attributed to the generation of more coherent spanwise vortical structures that transferred high momentum fluid from the outer boundary layer to the blade surface [21],[19].

As alternatives to the asymmetric electrode arrangement several researchers have proposed different electrode configurations with objective of improved control authority. Roy and Wang have proposed horseshoe and serpentine electrode configurations in a numerical study that showed promise for generating induced flows with three-dimensionality [22].

Plasma synthetic jet configurations have been proposed in both annular [24] [25] and linear configurations [27][28][32]. Santhanakrishnan and Jacobs experimentally studied both a steady and pulsed annular arrangement. Steady operation behaved like a synthetic jet in crossflow, and pulsed operation formed multiple counter-rotating vortex rings. Linear plasma synthetic jets were experimentally and numerically studied by Santhanakrishnan et al. in quiescent air using PIV [27]. The researchers found that similar findings as the annular array in that steady operation resulted in a zero-mass flux jet, and unsteady operation resulted in counter-rotating vortical structures. They also found a low peak velocity located close the actuator compared to the higher velocities observed with traditional synthetic jets.

Porter et al. [29][30] investigates improving upon the linear plasma synthetic jet by modifying the shape of the buried electrode to produce spanwise variation or "waviness" in the normal jet. They create spanwise waviness in the vertical jet by removing portions of the buried electrode (either diamond or square shapes) at specified spatial frequency. This limits the extent of the plasma to areas in which the bottom electrode has not been removed creating spanwise variation in the body force. They found that their electrode arrangements had the ability to generate vertical jets with spanwise spatial variation [30] .

The objective of alternative electrode configurations over the traditional linear plasma jet is generation of induced jets with three dimensionality and vorticity for enhanced boundary layer control. Jet vectoring is another interesting approach to generating increased vorticity and mixing by controlling the direction of the jet produced by linear plasma synthetic jets. Variations of jet vectoring have been suggested by Porter et al.[29][30], Bolitho and Jacobs[31], and Sherman[32]. The work of Porter et al. is very interesting in that they vary the voltage applied to each of the two exposed electrodes that form a linear plasma synthetic jet. They demonstrate ≈ +/- 60 degrees of jet directional control by varying the voltage between exposed electrodes. In addition they demonstrate oscillation of the jet by frequency modulation, greatly expanding the design space of linear plasma synthetic jets.

CURRENT STUDY

The three electrode configurations evaluated in the current work are shown in Figure 3. The first actuator configuration, DBD-01 was a spanwise array of 11 linear actuators spaced

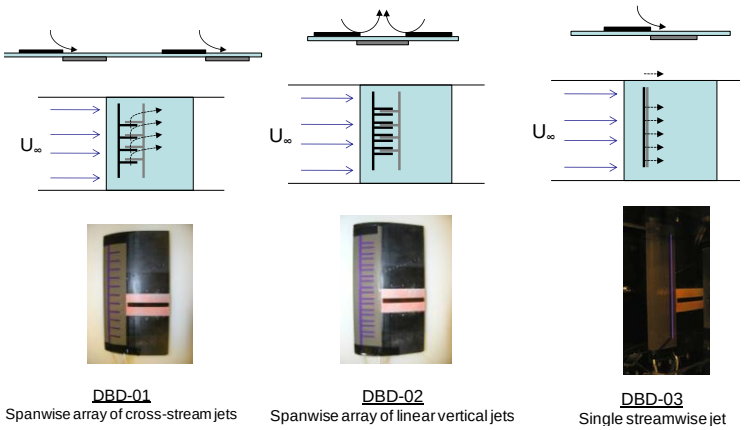

Figure 3. DBD Plasma Actuator Electrode Configurations.

20.6 mm on center, mounted parallel to the flow. This configuration produced an array of cross stream jets with the intent of generating longitudinal vorticity [43]. The second actuator, DBD-02 was a spanwise array of linear plasma synthetic vertical jets spaced 23.8 mm on center. Vertical jet arrangements can be created as annular or linear configurations, and operated steady or pulsed [24]-[28]. DBD-03 is a single asymmetric electrode across the span of the airfoil centered at 35% C_x. This type of geometry produces a downstream jet along the span of the airfoil.

Experimental Setup

Experiments were carried out in the AFRL Propulsion Directorate's LSWT facility 12" low speed wind tunnel. The straight section wind tunnel has a 30.5cm x 30.5cm x 61cm test section and an airspeed range of 4.5 – 65 m/s generated with a 7.5 kW electric motor. The inlet has a series of flow straighteners and turbulence-reducing screen followed by a 9.5:1 contraction providing an advertised turbulence level of less than 0.2%. The airfoil was mounted across the full span of the wind tunnel and had a 16.5cm chord length.

The E387 airfoil was rapid prototyped out of a polycarbonate ABS mixture. It is slightly modified in two ways. First a shallow cavity was created on the suction side of the airfoil to install a Surface Stress Sensitive Film (S3F) carrier. S3F is surface stress sensor used in this study to indicate shear stress. The S3F was formed external of the airfoil in the S3F carrier to ensure that it was smooth and flush with the surface of the carrier, and thus the surface of the airfoil. The S3F carrier was then installed into the cavity and held by either adhesive tape or countersunk screws near the trailing edge. The second modification to the airfoil is installation of surface pressure taps and plumbing. Due to the small thickness of the E387 (9.1%) the pressure tap lines (1.3mm diameter) were run along the pressure side of the airfoil and covered with tape. The modifications on the pressure side of the airfoil had little effect on the suction side boundary layer behavior, but as would be expected there is variation of drag along the span and an increase in drag over an unmodified airfoil.

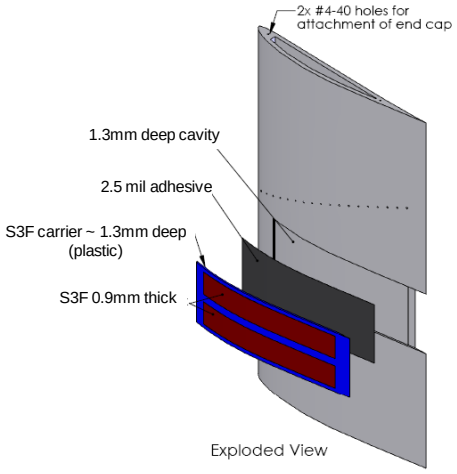

Figure 4. Modified E387 airfoil showing S3F mounting

Pressure coefficients, profile drag, shear direction by S3F, and flow visualization was obtained for each electrode configuration. An arrangement of AllSensor pressure transducers was used for pressure measurements with nominal 0.05% and maximum 0.25% linearity full scale. A 0-125 Pa (31.1 Pa/V) sensor was used for wake pressure measurements and inlet dynamic pressure. A 0-249 Pa (62 Pa/V) transducer was used for Cp measurements.

Drag was calculated by wake traverses using the method of Jones [42] using a Pitot-static probe located in a slot $0.5C_x$ downstream from the trailing edge.

$$C_d = \frac{2}{C_x}\int^{W} \frac{\sqrt{P_{T,w} - p_w}}{\sqrt{P_{T,in} - p_{in}}}\left(1 - \frac{\sqrt{P_{T,w} - p_{in}}}{\sqrt{P_{T,in} - p_{in}}}\right) dy$$

No corrections were applied to the data. Uncertainty in the Cp measurements is nominally 1.5% at the pressure minimum, and 3.1% in the trailing edge area at Re = $5x10^4$. At Re = 1.0 x 10^5 uncertainty in Cp is nominally 0.5% at the pressure minimum and 1.1% in trailing edge area. Uncertainty in the drag measurements omitting errors related to the probes is less than 1%.

Flow visualization was captured using a PCO 1600 camera and illuminated with a New Wave Solo 120 laser. The laser sheet was formed by Dantec sheet forming optics mounted to an articulating laser arm. The laser sheet thickness in this setup was ≈1 mm. The flow was seeded using water vapor generated from a Sussman 9 kW steam generator. The steam was injected in line with the wind tunnel approximately 2 meters upstream of the inlet. It should be noted that flow seeding will contaminate the plasma actuator, reducing its performance. The extent and uniformity of the plasma was affected by seeding contamination especially at lower voltage levels. Surface contamination from flow seeding was also noted in previous studies [26]. Flow visualization for each actuator was taken after wake traverse, Cp, and S3F data was acquired to minimize contamination.

S3F is a technique that enables the measurement of surface stresses over a wetted surface [23]. In many flows, both

pressure and shear fields can be measured simultaneously. The S3F technique consists of an elastic polymer film of known shear modulus and thickness applied to the surface being measured. The film deforms under to applied normal and tangential forces along the wetted interface. Film displacement is measured optically, then spatially cross-correlated with a wind-off image to obtain the two dimensional tangential displacement field. The normal force can be measured using the fluorescence signal emitted from a fluorescent probe embedded in the S3F. The shear stress and pressure gradients are calculated from the displacement field by solving the inverse problem using a finite element model of the elastic film [23]. The film has been used successfully for measurements in both high and low Reynolds number environments [23].

Previous experience using S3F at *low Reynolds number* has shown that it useful as a qualitative sensor and has potential as a quantitative sensor [38][38][39] [40]. In our low Reynolds number experiments very low shear modulus film is required (order of 100 Pa) to achieve adequate film sensitivity. Under a small pressure gradient the film displacement is linearly related to shear stress [23]. The raw film displacement vector field is an immediate indicator of surface shear direction. In a moderate and higher surface pressure gradient the raw displacement vectors are influenced by the pressure gradient as well as surface tangential stresses.

In this study the S3F tangential surface displacement was used as a direct indicator of shear stress direction. This is a valid assumption in flows with a small pressure gradient. Experiments have indicated that raw film tangential displacement near the E387 trailing edge reattachment can be shifted up to 2.5% axial chord by pressure gradient effect. Nonetheless it is deemed a worthwhile indicator of shifts in reattachment point for comparison of different actuator configurations tested in this study. In addition when S3F is applied in a filled cavity there will be an edge effect that decreases tangential displacement within several film thickness of the edge.

A PCO 4000 camera with 4008 x 2672 pixel resolution was used to obtain S3F flow-on and flow-off images. One strip of 0.9mm thick by 10mm wide S3F from C_x=42% to 98% was installed on the airfoil. The image field of view was 27.3mm x 18.2 mm with a magnification factor of 146.6 px/mm. Airfoil deformation and motion relative to the camera on the order 25-50 μm (3.5-7 pixels) was corrected for using 2D interpolation. Strips of patterned area just above and below the S3F rigidly fixed to the airfoil were used to correct for blade motion in each image pair.

Displacement maps were calculated using ISSI Inc. custom software that uses multipass optical flow to calculate displacement vectors. The displacement fields were then corrected for airfoil motion in Matlab. Accuracy of the optical flow technique used to calculate displacement vectors is better than 1/100 of a pixel [23]. In order to estimate the accuracy of the method used to correct for airfoil deformation a solid plastic filler panel was installed in place of the S3F. A fluorescent pattern was sprayed on the filler panel and flow-on and flow-off images were analyzed using the same process used for S3F images. For a series of 100 image pairs, correction for airfoil motion resulted in an average displacement field of +/- 0.015 pixels maximum. This is an indicator of the accuracy of the analysis method and airfoil motion correction technique, however, the actual accuracy is dependent on the pattern, signal to noise ratio, in addition to other factors.

Each electrode configuration was attached to the E387 airfoil using a uniform layer of 2 mil thick adhesive transfer tape. The DBD plasma actuators were fabricated in the U.S. AFRL Propulsion Directorate's thin film lab by photolithography and etching double-sided copper clad Kapton. The dielectric material was 5 mil thick Kapton with 1 oz copper (1.4 mil thick) electrodes. The top and bottom electrodes were formed flush with each other with no overlap. To assure the installation of the DBD plasma actuator on the airfoils did not trip the boundary layer, the actuators were wrapped completely around the leading edge of the airfoil. Only a 36 μm (1.4 mil) step up at the exposed electrode and an approximately 178 μm (7 mil) step down existed at the trailing edge of the actuator.

The electrodes were powered by two Titan Series power supplies from Compact Power. Each of the power supply output voltages were increased by an Industrial Test Equipment Co. transformer to kilovolt levels. In this work the DBD plasma actuators were operated in steady mode with continuous sinusoidal waveforms.

RESULTS AND DISCUSSION

Data was taken at four different Reynolds numbers with a focus here on performance at Re = 5 x 10^4, and Re = 1.0 x 10^5. At the lower Reynolds number the laminar boundary layer separates and large eddies are formed in the separated shear layer; the flow however, does not fully reattach. At the higher

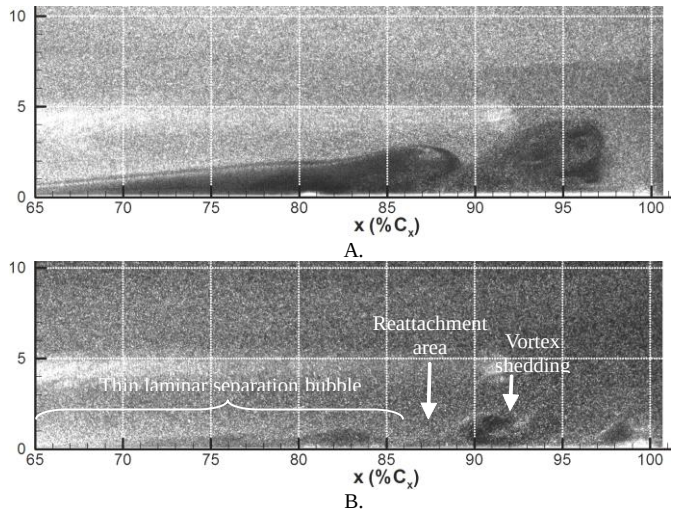

Figure 5. Flow visualization over the E387 suction surface from Cx = 67% to trailing edge with DBD-01 installed. Image A is at Re = 5 x 10^4. Image B is at Re = 1.0 x 10^5.

Reynolds number the boundary layer separates then transitions to turbulent and reattaches. The closed separation bubble sheds vortices which travel down the suction surface to the trailing edge. The large scale Kelvin-Helmholtz instabilities that develop in the separated shear layer lead to periodic vortex shedding observed in Figure 5B. Previous analysis has shown that time averaged measurements of the laminar separation look very similar to measurements of a traditional laminar separation bubble [33][34].

Figure 6 shows the suction surface Cp distribution with each plasma actuator installed at each Reynolds number tested along with inviscid results obtained in XFOIL [41]. The Cp distribution is consistent across each plasma actuator installed with regard to the presence of laminar separation without reattachment at Reynolds numbers tested below $6.0x10^4$, and laminar separation with reattachment for Reynolds numbers tested equal to $1.0x10^5$ and higher. Differences between the Cp profiles include higher peak Cp for DBD-01 than DBD-02 and DBD-03, with DBD-03 having the lowest peak Cp. In addition,

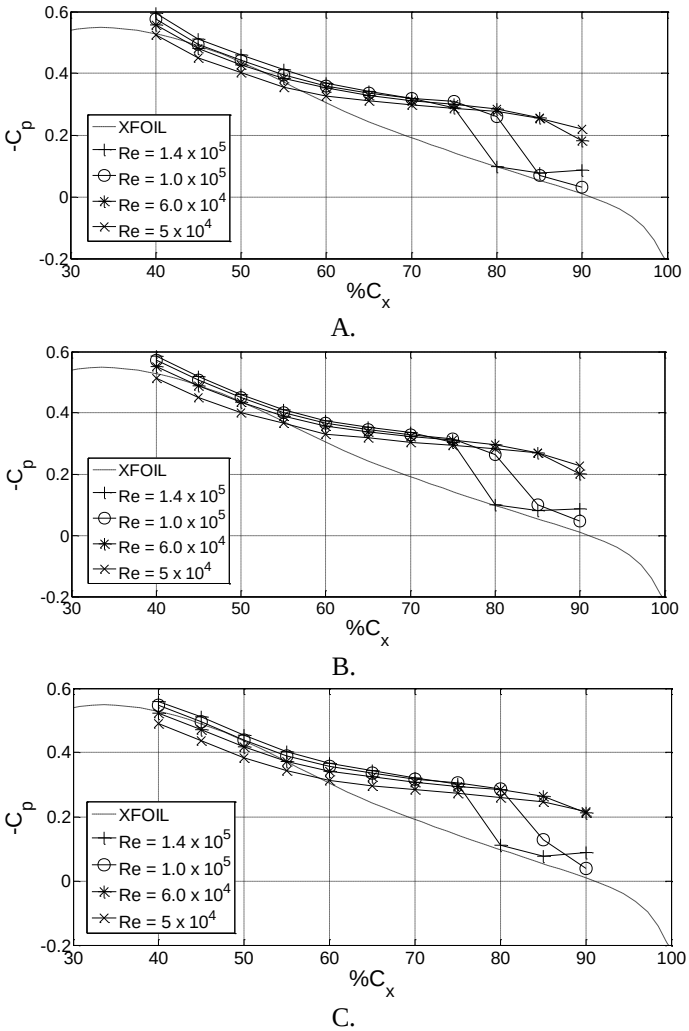

Figure 6. Suction surface Cp distribution with plasma actuators powered off. Plot A: DBD-01, B: DBD-02, C: DBD-03.

Cp plots indicate a difference in reattachment location for the three different plasma actuators tested. This difference is most noticeable in the Cp plot of DBD-03 at $Re=1.0x10^5$ in which the reattachment point noticeably shifts downstream 5% axial chord to Cx≈90%. It is important to keep in mind the spatial resolution of Cp data due to the limited amount of pressure taps. The S3F displacement field vector plots of Figure 9 indicate that the reattachment point is not uniform along the span, so a discrepancy of several percent axial chord is not unexpected. The difference in max Cp is likely due to the shift in mean reattachment location. The difference in data for each case is presumably due to two things: variation in the quality of installation of each plasma actuator, and the possibility that the electrode geometry caused small scale perturbations in the laminar boundary layer.

A summary of the separation and reattachment locations (extracted from Cp data) is provided in Figure 7 for each plasma actuator configuration tested.

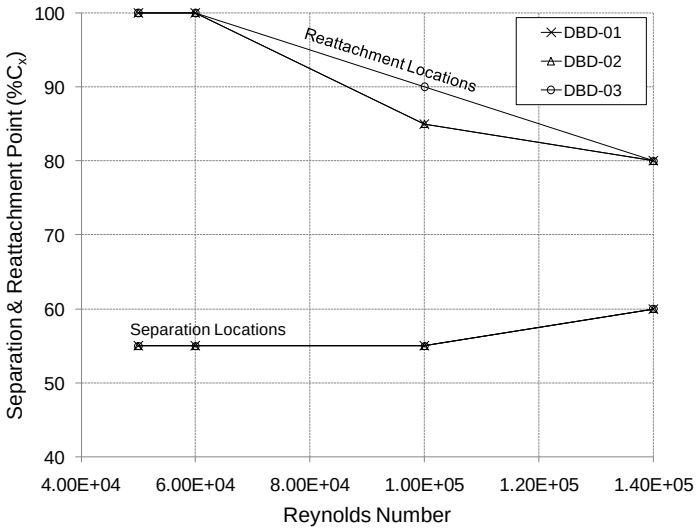

Figure 7. Mean suction surface separation and reattachment points for each plasma actuator configuration tested powered off.

Results at Re = 5 x 10^4

Cp and wake profile plots for each plasma actuator tested at a Reynolds number of $5x10^4$ are shown in Figure 8. A range of input voltages are shown in each plot. DBD-01 and DBD-02 drastically improve the surface pressure distribution with the time averaged measurements indicating flow reattachment. Powering on each actuator resulted in a significant narrowing of the airfoil wake. The wake of DBD-01 decreased in width as input voltage increased up to 5.6 kV_{pp} then increased width as voltage was amplified further. As the voltage of DBD-02 was increased beyond 4.2 kV_{pp} the wake gradually increased in width up to a voltage of 5.6 kV_{pp}. At input voltages above 5.6 kV_{pp} the wake began to narrow at its base with a significant increase in peak velocity deficit. Increasing the voltage of DBD-03 did not decrease the wake considerably beyond the lowest input voltage applied.

The use of S3F allows a unique view of the surface tangential displacement which directly corresponds to surface shear stress direction. Figure 9 is a series of mean surface tangential displacement vector plots obtained from S3F for DBD-01 actuator off and a range of applied plasma actuator voltage. The plots clearly show the effect of the plasma actuator. For actuator off conditions a strong reverse flow vortex is present at the trailing edge of the airfoil with a dead air region of separated flow just upstream from the vortex. As the plasma actuator is turned on the reverse flow vortex gradually shifts upstream with increase in voltage. There is a significant upstream shift and movement of the reverse flow vortex out of the view at the highest applied voltage of 7.2 kV_{pp}. At the highest voltage the mean flow appears to be reattached at $C_x \approx 93\%$ indicated by a zero crossing and downstream pointing displacement vectors. Figure 10 shows mean S3F tangential streamwise displacement for each plasma actuator tested at a spanwise location at $z = 5.5\%C_x$ (reference views in Figure 9). From Figs. 8-10 the following conclusions are made for operation at $Re=5 \times 10^4$:

DBD-01 – array of cross stream jets:

- Narrowing of the wake when the actuator is turned on indicates a decrease in drag and decrease in separation angle
- Mean S3F streamwise displacement in Figure 9 indicate that boundary layer reattachment and subsequent decrease in separated region does not occur until an applied voltage of 5.6 kV_{pp} and higher.
- Cp measurements agree with S3F in that there is no reattachment and/or minimal shift in reattachment point until higher actuator voltages are applied.

DBD-02 – array of vertical jets:

- Cp, S3F, and wake profile data all indicate that DBD-02 has a much larger effect on the flow at lower applied voltages compared to DBD-01.
- The reverse flow vortex moves upstream several percent chord when the plasma actuator is turned on at the lowest voltage. This is an improvement over DBD-01 and implies that the separated boundary layer is reattached or nearly reattached at the trailing edge at a voltage of 4.2 kV_{pp}. When the voltage is increased to 5.6 kV_{pp} the mean flow is clearly reattached as shown in the Cp and S3F data.

DBD-03 – downstream jet:

- DBD-03 has the least significant change in Cp distribution and S3F streamwise displacement when the actuator is turned on and voltage is increased.
- Decrease in wake profile at the lowest plasma actuator voltage indicates that there is an effect on the separated flow by the actuator.

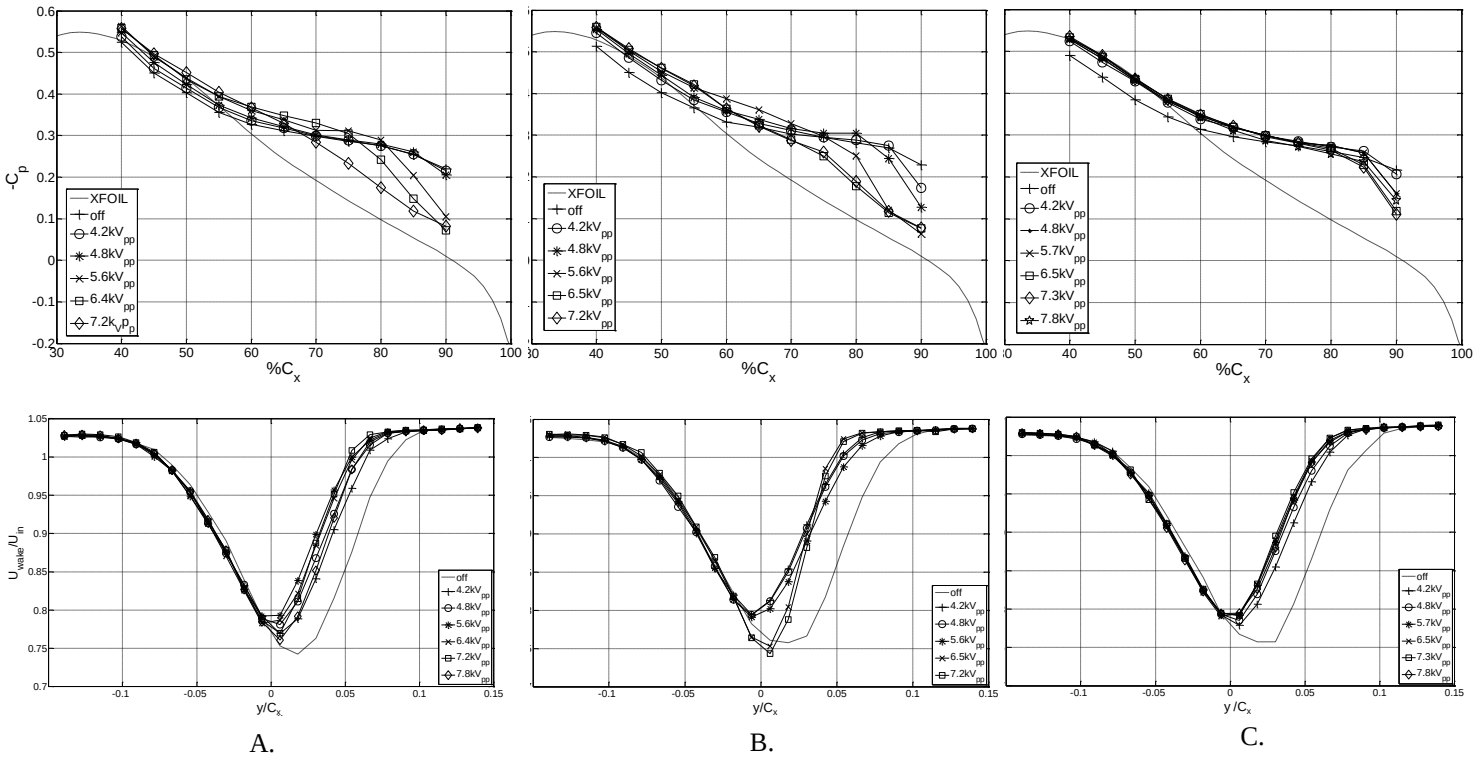

Figure 8. Suction surface Cp distribution and wake profile for each plasma actuator tested at 5 x 10^4. Column A: DBD-01, B: DBD-02, C: DBD-03.

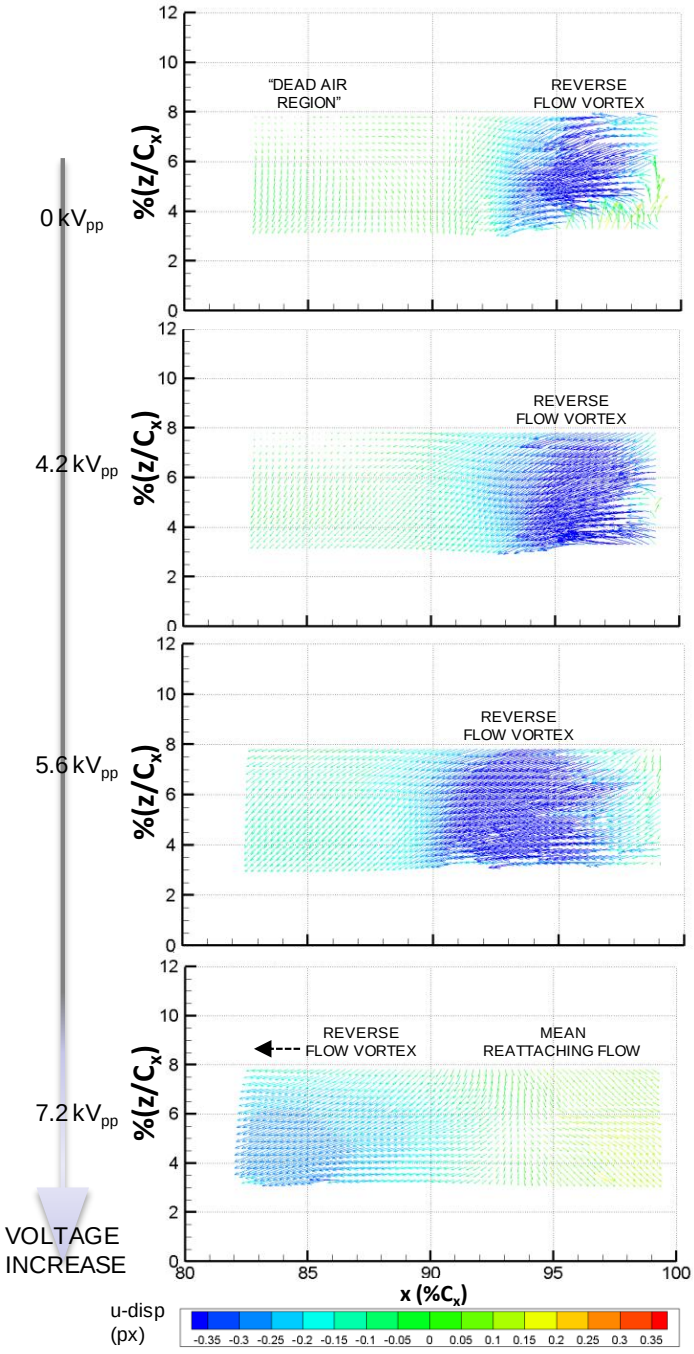

Figure 9. S3F measured surface tangential displacement of airfoil with DBD-01 installed. Flow speed is Re = 5 x 10^4 with various plasma actuator voltages

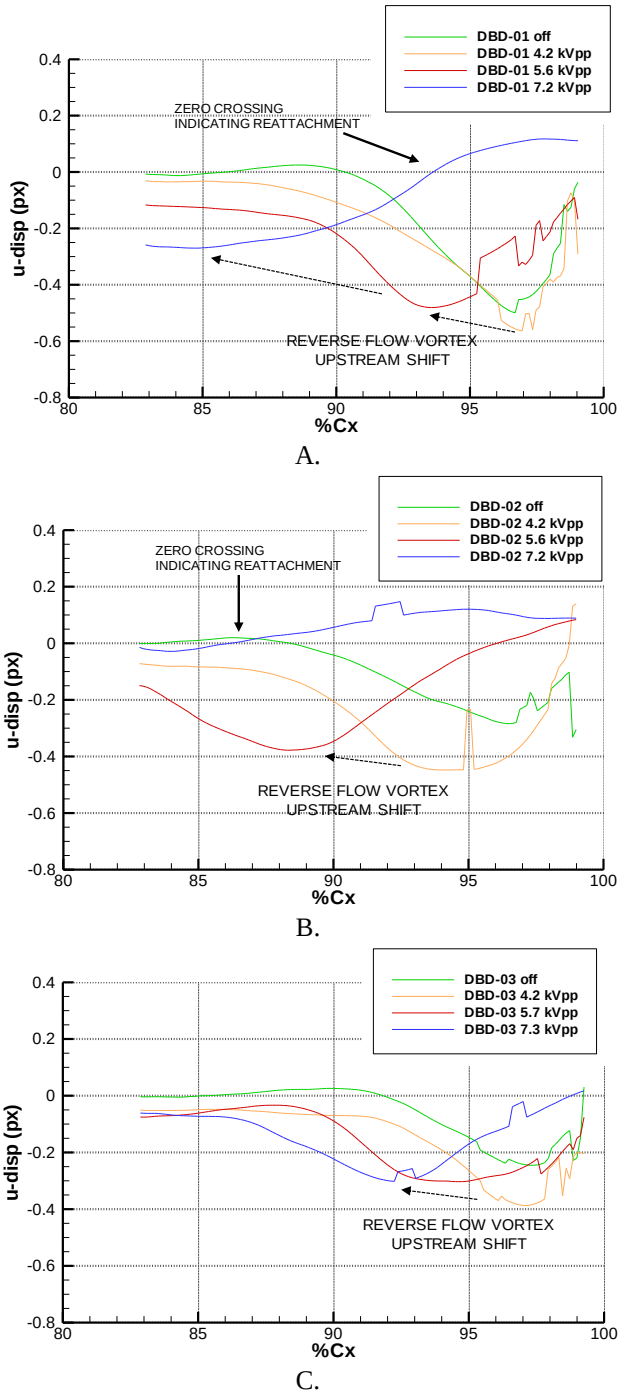

Figure 10. S3F streamwise disp. at Re = 5 x 10^4 & various plasma actuator voltages. Plot A: DBD-01, B: DBD-02, C: DBD-03.

Results at Re = 1.0 x 10^5

Figure 13 shows Cp and wake profiles at Re=1.0x10^5 for which there is laminar separation with reattachment when the actuator is powered off. The Cp profiles for each plasma actuator show an effect on suction surface Cp distribution when the actuator is turned on. The wake profiles (omitted here) however, show no decrease in wake width or depth with actuation; instead they remain constant or grow wider.

When the actuator is powered on the mean reattachment point gradually moves upstream as much as 5%C_x for DBD-01. The plateau region of the Cp distribution is flattened as voltage is increased for DBD-02 and DBD-03, first with a shift upstream of the reattachment point, then overall smoothing of

the pressure gradient. The S3F streamwise displacement in agrees with the Cp distributions in that there is a larger shift in reattachment point caused by DBD-02 and DBD-03, than for DBD-01. In fact, based on S3F data at the trailing edge and Cp data the mean flow reattaches far upstream of C_x=80% for DBD-02 with an applied voltage of 7.3 kVpp. This is a significant decrease in the extent of the mean separation bubble length. Earlier transition to turbulence with less dominance from large scale inviscid type instability and more viscous small scale turbulence in the boundary layer would support the increase in wake velocity deficit seen in DBD-02 at Re=1.0 x 10^5.

Based on the plots of Figures 11-13 the following conclusions are made for operation at Re = 1.0 x 10^5:

- All three plasma actuators move the mean reattachment point upstream as voltage is increased.
- Cp data indicates an upstream shift in reattachment point for DBD-01 of at least 5% Cx. S3F data indicates an upstream shift in mean reattachment of nearly 4% Cx at the S3F midpoint, but the reattachment point is not uniform in along the airfoil span.
- Cp data of DBD-02 shows a significant upstream shift in reattachment location as plasma actuator voltage is increased. The plateau in Cp that marks the separation bubble smoothes out significantly at an voltage of 6.5kVpp and above. The peak velocity deficit in the wake increases with voltage. S3F data shows a significant upstream shift in mean reattachment location as the voltage is increased culminating with a reattachment point upstream of the view which ends at C_x=83%.

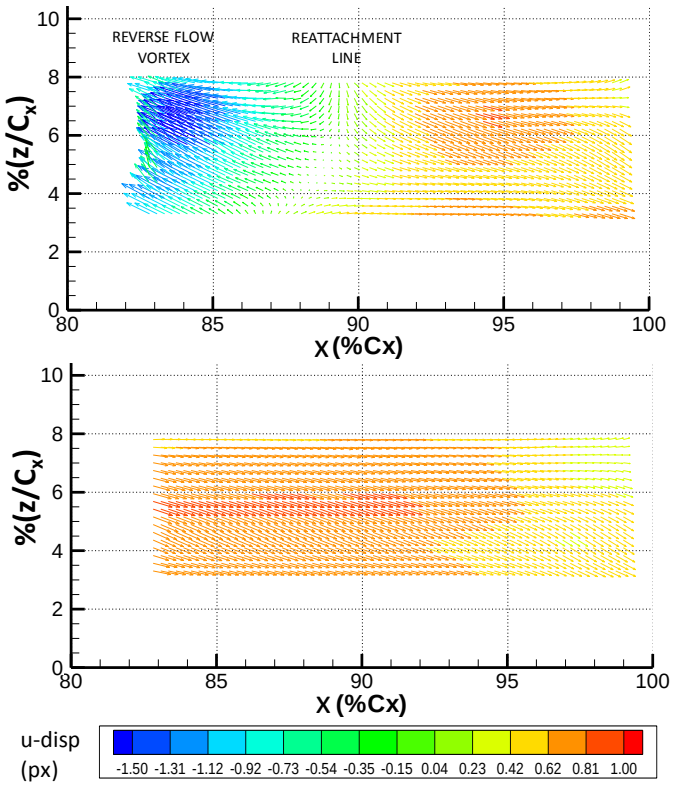

Figure 11. S3F tangential displacement of DBD-02 at Re = 1.0 x 10^5 for Top: Actuator off, Bottom: 7.2 kVpp.

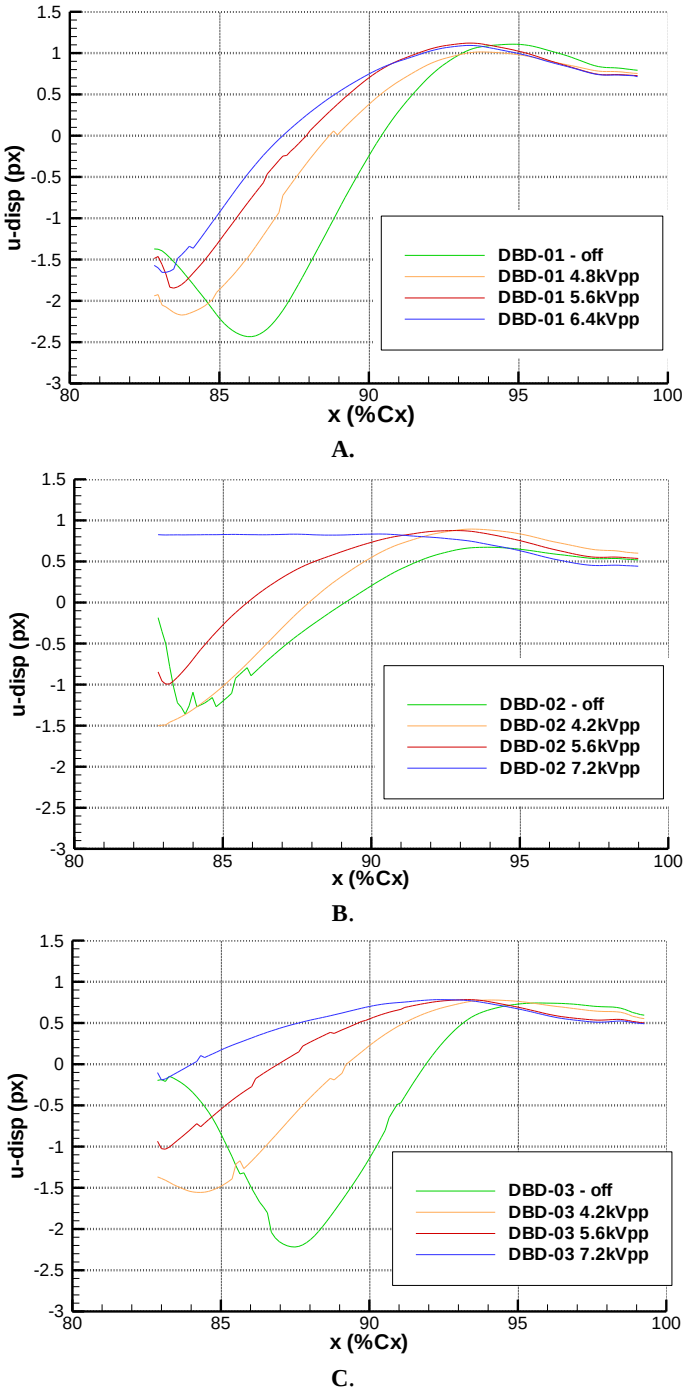

Figure 12. S3F tangential displacement at Re = 1.0 x 10^5 and various plasma actuator voltages. Plot A: DBD-01, B: DBD-02, C: DBD-03.

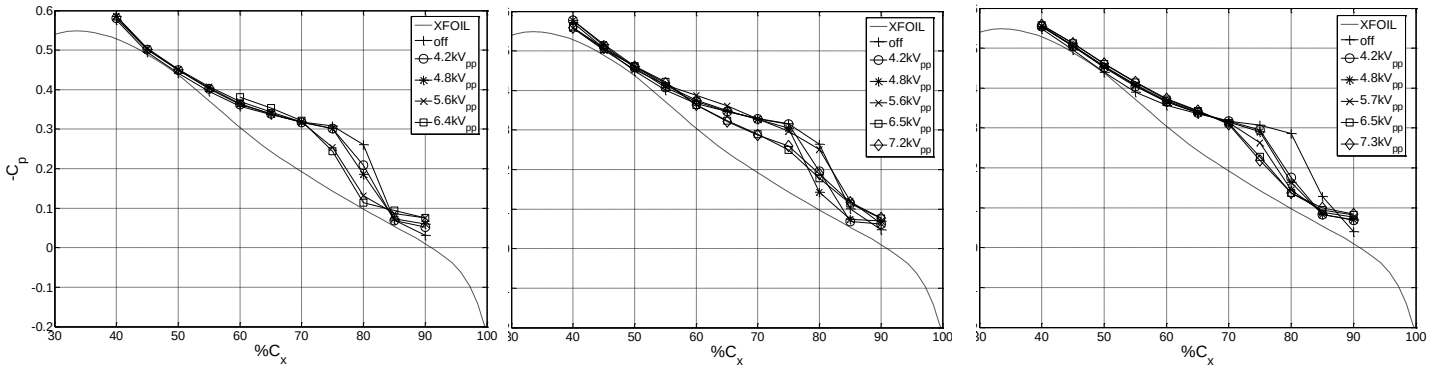

Figure 13. Suction surface Cp distribution and wake profile for each plasma actuator tested at 1.0 x 10^5. Column A: DBD-01, B: DBD-02, C: DBD-03.

- Powering on plasma actuator DBD-03 shifts the reattachment point upstream with increases in voltage providing further upstream shift in reattachment. S3F indicates a nearly 8% upstream shift in mean reattachment point as voltage is increased to 7.3 kVpp.

Discussion

Each actuator clearly had an effect on suction surface laminar boundary layer separation as summarized in the plots of Figure 14 that show the S3F indicated mean reattachment points. At the lower Reynolds number $5.0x10^4$ in which there was laminar separation without reattachment, powering on actuators DBD-01 and DBD-02 clearly resulted in a significant upstream shift in mean reattachment location. Electrode configuration DBD-02, the spanwise array of linear vertical jets led the actuators tested with reattachment at Cx=87%. This is confirmed by Cp data that shows significant smoothing of the plateau in pressure gradient that marked flow separation. DBD-03 did not definitively result in mean reattachment at the highest voltage tested, but did result in a significant decrease in wake width when the actuator was powered. It is possible that higher plasma actuator voltage would have resulted in mean reattachment.

At the higher Reynolds number, $1.0x10^5$, laminar boundary separation with mean reattachment was present with the plasma actuator off. In these flow conditions powering on DBD-03 significantly shifted the mean reattachment line upstream 8%Cx. Less of an upstream shift was observed for DBD-01, the spanwise array of cross stream jets, however S3F data was not obtained at 7.2kVpp to compare to the other actuators, and further upstream shift may have resulted. Electrode configuration DBD-02 had the largest apparent effect with an S3F indicate shift in mean reattachment point beyond the field of view (reattachment at Cx<83%).

Drag data is presented in Figure 15 for each actuator tested. Powering on each actuator resulted in a decrease in drag at $Re=5x10^4$, with each actuator reaching a minimum drag value. DBD-02, the spanwise array of linear vertical jets reached its minimum at the lowest plasma actuator voltage, with a 33% reduction in drag. DBD-03 the downstream facing jet also had a significant decrease in drag 30% at $Re=5.0x10^4$. At the $Re=1.0x10^5$ powering on the actuators did not result in a decrease in drag. In fact the drag gradually increased with increase in voltage for each actuator. This is most likely due to the increased length of turbulent boundary layer as the separation bubble decreases in length, resulting in no improvement in drag. The drag plot shown in Figure 15 also displays the difference in drag due to variation in the quality of installation of each plasma actuator on the airfoil. The airfoil with DBD-03 has the largest initial drag when the plasma actuator is powered off.

Flow visualization images are shown in Figs. 16-19 in order to further understand the effect of each actuator. Figure 16 shows a large decrease in separation and boundary layer thickness as the actuator power is increased. The effect of the actuator at lower voltage settings is decrease in separation angle and smaller, less dominate large scale inviscid structures in the separated shear layer. At the higher voltage a thin separation bubble is formed. This explains the earlier minimum observed in drag. As the voltage increases past 5.6 kV_{pp} and the separated boundary layer reattaches, no additional gains are made in drag due to increased turbulent boundary layer length.

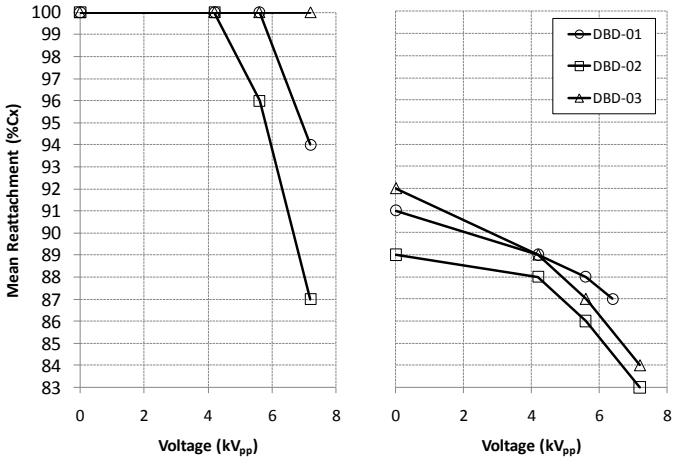

A. Re= $5x10^4$ B. Re = $1.0x10^5$

Figure 14. S3F indicated shifts in mean reattachment locations with increase in voltage.

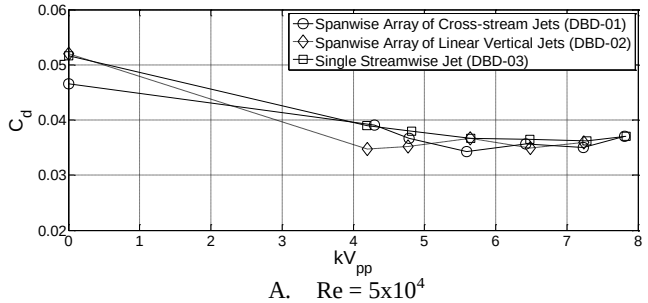

A. Re = $5x10^4$

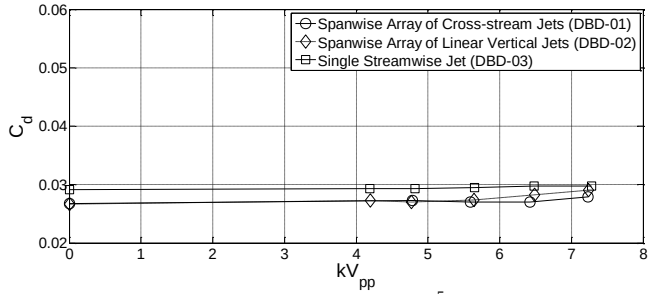

B. Re = 1.0×10^5

Figure 15. Drag for each actuator tested.

In Figure 17 flow visualization in the area of the plasma actuator and boundary layer separation is shown. The actuator on image is very interesting and shows eddies formed downstream of the actuator. The laser sheet in this case was placed centered with one of the plasma actuator vertical jets. The eddies were only observed at the highest voltage tested 7.3 kV_{pp}. The linear vertical jet is aligned with the streamwise direction and is expected to introduce three dimensional vorticity by creating a local separation region. This bottom image in Figure 17 clearly shows that, at the least spanwise coherent eddies form entraining higher momentum flow from the freestream to the wall.

The effect of plasma actuator DBD-03 at the trailing edge is shown in Figure 18. This plasma actuator was least effective at the lowest Reynolds number tested. The flow visualization indicates that as voltage is increased the separated shear layer develops into a boundary layer with large scale streamwise structures. This orientation acts as a wall jet entraining momentum from the freestream and adding momentum to the boundary layer. The flow visualization in this study indicates the configuration was less effective at promoting transition and reattachment of the boundary layer. The large scale inviscid structures are maintained and do not appear to break up into small scale structures. It did however, decrease drag by 30%. At the higher Reynolds number of Re=$1.0x10^5$ in which a mean reattaching separation bubble was present in the actuator off case, the plasma actuator DBD-03 was very effective at moving the reattachment point upstream (see Figure 19).

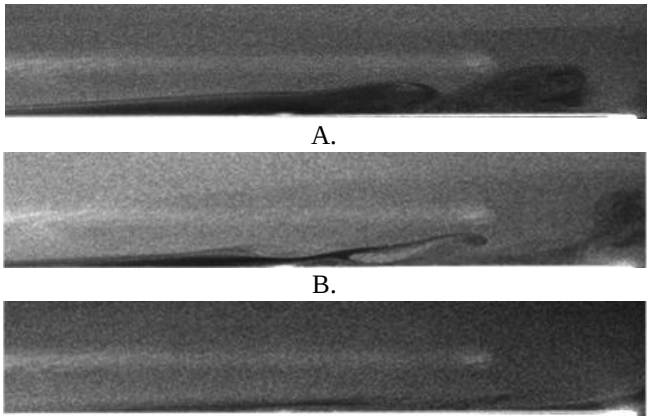

A.

B.

C.

Figure 16. Flow visualization of plasma actuator DBD-01 at the trailing edge from Cx=65% to 101% at a Re = 5 x 10^4. Image A: actuator off, B: 5.6 kV_{pp}, C: 7.2 kV_{pp}

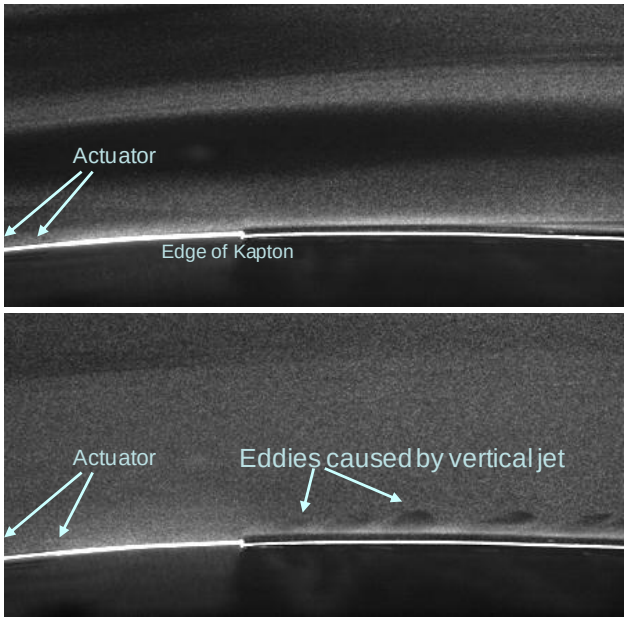

Figure 17. Flow visualization showing spanwise coherent unsteadiness generated by the vertical jets of DBD-02 with Re=$5x10^4$. Top: actuator off, Bottom: actuator voltage 7.2 kVpp. View is from approximately Cx=30% to 60%.

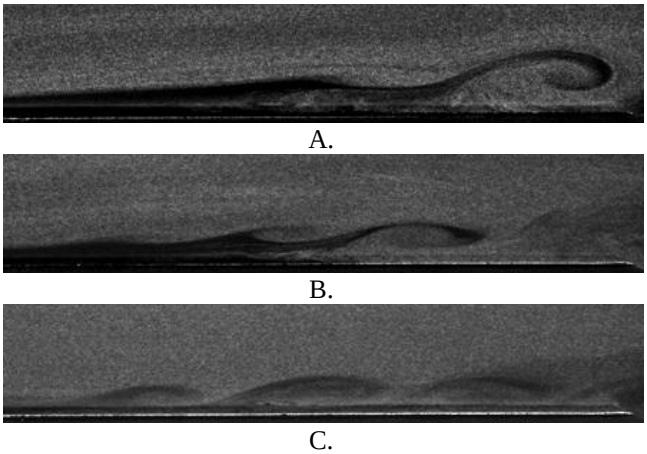

A.

B.

C.

Figure 18. Flow visualization of plasma actuator DBD-03 at the trailing edge from Cx=70% to 101% at a Re = 5 x 10^4. Image A: actuator off, B: 4.8 kV_{pp}, C: 7.2 kV_{pp}

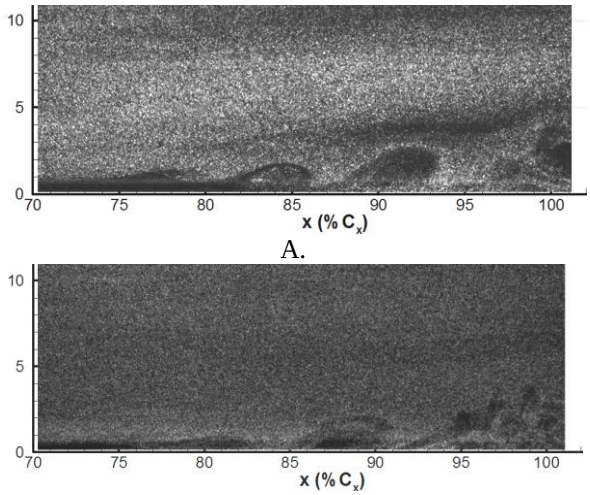

Figure 19. Flow visualization of airfoil with plasma actuator DBD-03 installed. Suction surface near trailing edge is shown at Re=1.0x10^5. Image A: actuator off, B: 7.3 kV$_{pp}$.

CONCLUSIONS

Three different plasma actuator electrode configurations were compared for use in a low Reynolds number separation control system. Two of the actuator configurations were implemented with the intent of generating three-dimensional, or streamwise vorticity to improved moment entrainment from the freestream into the boundary layer. Operation at two different Reynolds numbers was presented here. At the lower Reynolds number of 5x10^4, laminar separation without reattachment was observed with the actuators powered off. At the higher Reynolds number 1.0x10^5 the boundary layer separated and then reattached prior to the trailing edge.

Three parameters were used to compare the performance of each actuator: Suction surface Cp profile, S3F streamwise surface displacement, and drag. At the lowest Reynolds number tested, S3F reattachment locations indicated plasma actuator DBD-02, a spanwise distributed array of linear vertical jets, reattached the flow and moved the mean reattachment upstream as voltage was increased to 7.2kV$_{pp}$. This configuration also resulted in the largest improvement in drag.

At the higher Reynolds number each plasma actuator moved the reattachment point upstream. Plasma actuator configuration DBD-02 shifted the reattachment point upstream in excess of 6% Cx, likely significantly further as the mean reattachment point moved out of the field of view. Plasma actuator configuration DBD-03 shift the reattachment point upstream 8% Cx. Each actuator tested at Re=1.0x10^5 showed an increase in drag as the separation length decreased with increased voltage. This is considered to be due to an increase in turbulent boundary layer length.

Several conclusions can be made from the results of this study:

1. The spanwise distributed array of linear vertical jets (DBD-02) are deemed the most effective in the two flow conditions presented here. However, plasma actuator DBD-01, a spanwise array of cross-stream jet showed promise and it is possible that a different spanwise spacing of the jets would yield better results.
2. Alternative DBD plasma actuator electrode configurations to the standard asymmetric electrode configuration must be considered and studied in more detail as they show potential for performance improvements.
3. The electrode configuration that will provide the most effective separation control at low Reynolds number will likely change with flow conditions. This points towards electrode configurations and power electronics that enable induced velocity jet vectoring. A configuration that uses jet vectoring could create the effects of configurations DBD-01, and DBD-02, and enable switching between jet orientations based on flow condition.

It should be mentioned that the success of the two spanwise distributed arrays, used here in hopes of generating three dimensionality and streamwise vorticity, point towards the conclusion that longitudinal vorticity was generated. However, further study is necessary to verify the control mechanism that led to reattachment.

ACKNOWLEDGMENT

The authors would like to thank Dr. Richard Rivir for the use of a substantial amount of the test and measurement equipment used for this work. Dr. Sergey Fonov and his coworkers at Innovative Scientific Solutions Inc. are acknowledged for fabricating the S3F used in this work and training and assistance on the use of S3F technology. Thank you to Dr. Rivir, and Dr. Joseph Shang for sharing their knowledge of DBD plasma actuators with the lead author.

REFERENCES

[1] Lake, J., "Flow Separation Prevention on a Turbine Blade in Cascade at Low Reynolds Number" PhD Dissertation, Air Force Institute of Technology, 1999.

[2] Mahmood, G., Hill, M., Nelson, D., "Local Heat Transfer and Flow Structure On and Above a Dimpled Surface in a Channel", ASME 2000-GT-230, 2000.

[3] Sondergaard, R., Rivir, R., Bons, J., "Control of Low-Pressure Turbine Separation Using Vortex-Generator Jets," *Journal of Propulsion and Power, 18,* 2002, pp. 889-895.

[4] Bons, J., Sondergaard, R., Rivir, R., "Turbine Separation Control Using Pulsed Vortex Generator Jets," *Journal of Turbomachinery, 123*, 2001, pp. 198-206.

[5] Johnston, J. P., and Nishi, M., "Vortex-Generator Jets: Means for Flow Separation Control," *AIAA Journal, 28,* 1990, pp. 989-994.

[6] Moreau, E., "Airflow control by non-thermal plasma actuators", *Journal of Physics D: Applied Physics, 40,* 2007, pg 605-636.

[7] Enloe, C., McLaughlin, T., VanDyken, R., Kachner, K., Jumper, E., Corke, T., "Mechanisms and Responses of a Single Dielectric Barrier Plasma Actuator: Plasma Morphology" AIAA Journal V. 42, No. 3, pp 589-594 2004.

[8] Enloe, C., McLaughlin, T., VanDyken, R., Kachner, K., Jumper, E., Corke, T., Post, M., Haddad, O. "Mechanisms and Responses of a Single Dielectric Barrier Plasma Actuator: Geometric Effects." AIAA Journal V. 42, No. 3, pp. 595-604 2004.

[9] Enloe, C., McLaughlin, T., Baughn, J., "Parameterization of Temporal Structure in the Single-Dielectric-Barrier Aerodynamic Plasma Actuator", AIAA Journal, 44, pp. 1127-1136, 2006.

[10] Rivir, R., White, A., Carter, C., Ganguly, B., Jacob, J., Forelines, A., Crafton, J., "AC and Pulsed Plasma Flow Control, AIAA Paper No. AIAA-2004-847, January, 2004.

[11] Pons, J., Moreau, E., and Touchard, G., "Asymmetric surface barrier discharge in air at atmospheric pressure: electric properties and induced airflow characteristics", *Journal of Phy. D: Appl. Phys., 38*, pg 3635-3642.

[12] Fridman, A., Chirokov, A., and Gutsol, A., "Non-thermal atmospheric discharges", *Journal of Physics D: Applied Physics, 38*, 2005, R1-R24.

[13] Roth, J., Sherman, D., and Wlidkenson, S., "Boundary Layer Flow control with a One Atmosphere Uniform Glow Discharge Plasma," Paper No. AIAA-1998-0328, January 1998.

[14] Porter, C., Baughn, J., McLaughlin, T., Enloe, C., Font, G. "Plasma Actuator Force Measurements" AIAA Journal, V. 45, July 2007, pg 1562-1570.

[15] Sondergaard, R., Rivir, R., Bons, J., "Control of Low-Pressure Turbine Separation Using Vortex-Generator Jets", *Journal of Propulsion and Power, 18*, pp. 889-895, 2002.

[16] Shang, J., Personal Correspondence, July 2008.

[17] Rivir, R.B., Sondergaard, R., Bons, J.P., and Yurchenko, N. 2004. Control of Separation in Turbine Boundary Layers, AIAA Paper No. 2004-2201.

[18] Huang, J., Corke, T., and Thomas, F., "Plasma Actuators for Separation Control of Low Pressure Turbine Blades", AIAA Paper No. 2003-1027, January, 2003.

[19] Huang, J., Corke, T., and Thomas, F., 2006. "Unsteady Plasma Actuators for Separation Control of Low-Pressure Turbine Blades", AIAA Journal, 44, pp. 1477-1487.

[20] Rizzetta, D.P. and Visbal, M.R., "Simulation of Plasma-Based Flow-Control Strategies for Transitional Highly Loaded Low-Pressure Turbines", AIAA Paper No. AIAA-2007-938, June, 2007.

[21] Rizzetta, D. P., and Visbal, M. R., "Numerical Investigation of Plasma-Based Flow Control for Transitional Highly Loaded Low-Pressure Turbine" *AIAA Journal, 45*, pp. 2554-2564, 2007.

[22] Roy, S., and Wang, C., "Bulk flow modification with horseshoe and serpentine plasma actuators", J. Phys. D: Appl. Phys. 42 (2009), pp. 1-5.

[23] Crafton, J., Fonov, S., Forlines, A., Goss, L., "Skin Friction Measurements Using Elastic Films", *AIAA Aerospace Sciences Meeting*, AIAA, Orlando, FL, 2010, AIAA-2010-42.

[24] Jacob, J., Ramakumar, K., Anthony, R., Rivir, R., "Control of Laminar and Turbulent Shear Flows Using Plasma Actuators" *4th International Symposium on Turbulence and Shear Flow Phenomena*, Williamsburg, VA June 27-29, 2005.

[25] Santhanakrishnan, A., and Jacob, J., "Flow Control with Plasma Synthetic Jet Actuators" *J. Phys. D: Appl. Phys. 40* (2007) pp 637-651.

[26] Santhanakrishnan, A., and Jacob, J., "Effect of Plasma Morphology on Flow Control Using Plasma Synthetic Jet Actuators" AIAA Paper No. 2007-783.

[27] Santhanakrishnan, A., and Jacob, J., "Characterization of Linear Plasma Synthetic Jet Actuators". AIAA Paper No. 2008-538.

[28] Santhanakrishnan, A., Reasor, J., and Lebeau, R. "Characterization of linear plasma synthetic jet actuators in an initially quiescent medium". *Physics of Fluid 21*, 2009, DOI:10.1063/1.3097004.

[29] Porter, C., Abbas, A., Cohen, K., McLaughlin, T., and Enloe, C., "Spatially Distributed Forcing and Jet Vectoring with a Dielectric Barrier Discharge Plasma Actuator," AIAA Paper No. 2008-1374.

[30] Porter, C., Abbas, A., Cohen, K., McLaughlin, T., Enloe, C., "Spatially Distributed Forcing and Jet Vectoring with a Plasma Actuator" *AIAA Journal, 47*, (2009), pp. 1368-1378.

[31] Bolitho, M., and Jacob, J., "Thrust Vectoring Flow Control Using Plasma Synthetic Jet Actuators," AIAA Paper No: 2008-1368.

[32] Sherman, D. M. "Manipulating Aerodynamic boundary layers using an electrohydrodynamic effect generated by a One Atmosphere Uniform Glow Discharge Plasma", August 1998, Master's Thesis, University of Tennessee, Knoxville, p. 52.

[33] Lin, J. C. and Pauley, L. L., "Low-Reynolds Number Separation on an Airfoil," *AIAA Journal, 34*, pp. 1570-1577.

[34] Selig M. S. and Mcgranahan, B. D., "Wind Tunnel Aerodynamic Tests of Six Airfoils for Use on Small Wind Turbines." National Renewable Energy Laboratory Subcontractor Report, NREL/SR-500-34515, 2004.

[35] List, J., Byerley, A., McLaughlin, T., Van Dyken, R., "Using a Plasma Actuator to Control Laminar Separation on a Linear Cascade Turbine Blade", *41st Aerospace Sciences Meeting*, AIAA Paper No. AIAA-2003-1026.

[36] McQuilling, M., Wolff, M., Fonov, S., Crafton, J., Sondergaard, R., "An Experimental Investigation of a Low-Pressure Turbine Blade Suction Surface Using a Shear and Stress Sensitive Film", *Experiments in Fluids*, V. 44, No. 1, pp. 73-88.

[37] McQuilling, M., Wolff, M., Fenov, S., Crafton, J., and Sondergaard, R., "An Experimental Investigation of Suction Surface Flow Features on a High-Lift LPT", AIAA Paper No. 2008-79.

[38] McQuilling, M., Wolff, M., Fonov, S., Crafton, J., Sondergaard, R., "An Experimental Investigation of a Low-Pressure Turbine Blade Suction Surface Using a Shear and Stress Sensitive Film", *Experiments in Fluids*, V. 44, No. 1, pp. 73-88.

[39] McQuilling, M., Wolff, M., Fenov, S., Crafton, J., and Sondergaard, R., "An Experimental Investigation of Suction Surface Flow Features on a High-Lift LPT", AIAA Paper No. 2008-79.

[40] Marks, C., Nessler, C., Sondergaard, R., Wolff, M., Crafton, J., Fonov, S., "High Lift LPT Blade Suction Surface Flow Investigation Using Surface Stress Sensitive Film, *45th AIAA Joint Propulsion Conference & Exhibit*, AIAA Paper No. 2009-5106, Denver, CO, 2009.

[41] Drela, M., and Youngren, H., 2001. XFOIL 6.9 User Primer. Accessed on January 4, 2009. http://web.mit.edu/drela/Public/web /xfoil/xfoil_doc.txt

[42] Goett, H., "Experimental Investigation of the Momentum Method for Determining Profile Drag," NACA Report No. 660, 1939.

[43] Roth, J., Sherman, D., and Wilkinson, S., "Electrohydrodynamic Flow Control with a Glow-Discharge Surface Plasma," *AIAA Journal, 38*, pp. 116.